

CALIBRATION AND VALIDATION OF ALOS/AVNIR-2

- Generation of RPC Model and Land Cover Classification -

PI No 229

Masayuki MATSUOKA¹

¹Agricultural Unit, Kochi University

1. INTRODUCTION

Advanced Visible and Near Infrared Radiometer type 2 (AVNIR-2) onboard ALOS has been accumulating the observation data over land. Long-term acquisition is expected for the purpose of monitoring the land cover at global scale. Geometric and radiometric quality of remote sensing products are great interests of users, because these affect the accuracy of the analytical results. The purposes of this study are assessment of geometric accuracy of AVNIR-2, and the feasibility study of data application for the land cover classification.

The first part of this report is the geometric accuracy assessment. Rational polynomial coefficient (RPC) model of AVNIR-2 are generated and used for the geometric rectification of the image. The positional error is evaluated and corrected by means of modification of RPC model using ground control points (GCPs).

The second part is the land cover classification of tropical forest in Malaysia using AVNIR-2. Multispectral image is segmented to the small regions by region growing method. Identification of land cover type, subsequently, is carried out based on decision tree classification scheme. Post classification is applied to correct the misclassification.

2. DATA

Level 1B1 products of AVNIR-2 is used in this study because it is not geometrically corrected and orbital information is available by each line of image. This is necessary to generate the RPC model in this study. Products are listed in table 1, and observation areas are shown in figure 1.

Four products over Kanto area in Japan with different pointing angle were used for RPC model generations. This is for the purpose of assessment of geometric accuracy along with pointing angle setting. Band 3 is used for this analysis because it is the base band of sensor geometry of AVNIR-2 [1].

One product over Malaysian tropical forest is used for land cover classification. All of four bands are applied in this analysis. RPC model, which is derived from above mentioned analysis, was used for the geometric correction of this scene, and it is modified based on the GCPs that were corrected on the logging roads by GPS. The image was geometrically rectified to latitude-longitude projection with 10 meters spatial resolution.

Table 1 Products used in this study

Purpose*	Pointing angle	Observation date	Scs_SceneID
a	-41.5	Mar. 10, 2007	ALAV2A059802900
a	-21.5	Apr. 06, 2007	ALAV2A063742890
a	0.0	Mar. 01, 2007	ALAV2A058492880
a	34.3	Oct. 17, 2006	ALAV2A038802850
b	0.0	May 24, 2007	ALAV2A070753540

* a: Geometric accuracy assessment, b: land cover classification

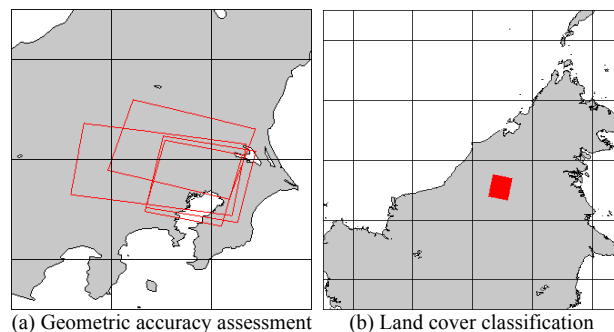


Fig. 1 Observation areas

3. METHODOLOGIES

3.1 Generation of RPC model

The RPC model is the alternatives of the physical model of sensor geometry, and generalized formulas that can convert geographic locations (latitude, longitude and height) to pixel position (line and pixel position in the image) without any mechanical parameters of the sensor. Therefore, the images are ortho-rectified easily using RPC model and digital elevation model (DEM). The RPC model of AVNIR-2 is generated from level 1B1 products by means of geometric and orbital information of AVNIR-2.

The equation of the RPC model in this study is shown in equations 1. The formula is based on NITF version 3 [2] in order to keep the usability in generic remote sensing software.

$$l' = \frac{N_l(\phi', \lambda', h')}{D_l(\phi', \lambda', h')}, \quad (1-a)$$

$$p' = \frac{N_p(\phi', \lambda', h')}{D_p(\phi', \lambda', h')} \quad (1-b)$$

where

$$\begin{aligned}
N_l(\phi', \lambda', h') = & c_0 + c_1 \lambda' + c_2 \phi' + c_3 h' + c_4 \lambda' \phi' + c_5 \lambda' h' + c_6 \phi' h' \\
& + c_7 \lambda'^2 + c_8 \phi'^2 + c_9 h'^2 + c_{10} \lambda' \phi' h' + c_{11} \lambda'^3 + c_{12} \lambda' \phi'^2 \\
& + c_{13} \lambda' h'^2 + c_{14} \lambda'^2 \phi' + c_{15} \phi'^3 + c_{16} \phi' h'^2 + c_{17} \lambda'^2 h' \\
& + c_{18} \phi'^2 h' + c_{19} h'^3
\end{aligned} \tag{1-c}$$

$D_l(\phi', \lambda', h')$, $N_p(\phi', \lambda', h')$ and $D_p(\phi', \lambda', h')$ are the same form as $N_l(\phi', \lambda', h')$, and c_0 equals to one in $D_l(\phi', \lambda', h')$ and $D_p(\phi', \lambda', h')$. l' , p' , ϕ' , λ' and h' are normalized values as follows:

$$l' = (l - \text{offset}_l) / \text{scale}_l \tag{1-d}$$

$$p' = (p - \text{offset}_p) / \text{scale}_p \tag{1-e}$$

$$\phi' = (\phi - \text{offset}_\phi) / \text{scale}_\phi \tag{1-f}$$

$$\lambda' = (\lambda - \text{offset}_\lambda) / \text{scale}_\lambda \tag{1-g}$$

$$h' = (h - \text{offset}_h) / \text{scale}_h \tag{1-h}$$

where

l : Line number in the image

p : Pixel number in the image

ϕ : Latitude in degrees

λ : Longitude in degrees

h : Height from the earth ellipsoid in meters

Five pairs of "scale" and "offset" are decided scene by scene to normalize the value ranges, that is, maximum should be 1, and minimum is -1. Totally, 38 coefficients are derived by least square estimation. This estimation is achieved by the direct solution based on the terrain-independent computation scenario [3] in this study. The data sample used for the estimation, i.e. pairs of (latitude, longitude, height) and (line, pixel), are acquired by following steps. The schematic diagram of sample derivation is shown in figure 2.

Step 1: arrangement of three-dimensional grid

The grid is assigned along the axis of line, pixel and height. Latitude and longitude are computed for each grid points in step 2. Grid intervals are 1600 and 1420 for line and pixel direction respectively, due to the image size. For height, grid is set by 2000 meters step from -1000 to 9000 in reference to the range of earth elevation. This density of grid was decided by previous analysis of estimation stability and computational load.

Step 2: Derivation of latitude and longitude

Latitude and longitude of grid points are derived using geometric equation and orbital information recorded in the product. Firstly, position at 0 meter height is computed by "Level 1B1(pixel, line), (latitude, longitude) transformation coefficients" for each band in the leader file of the product. Secondary, satellite position at each grid is computed by the interpolation of orbital information in the trailer file. Hermite interpolation was applied in this study. Thirdly, line of sight vector is derived

from satellite and ground position. Finally, ground position at each ellipsoidal height is computed by computing the intersection point of line of sight vector and height-added earth ellipsoid.

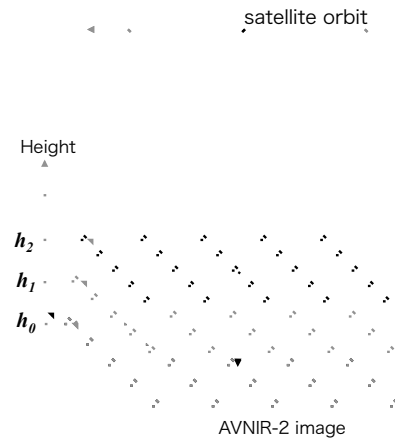


Fig. 2 Terrain-independent scenario

Since level 1B1 products of AVNIR-2 is not geometrically rectified, staggered arrayed detector (figure 3) is not corrected [4], and image is out of alignment by even and odd detectors. This induces approximately 5 pixels displacement on the ground at nadir (pointing angle is 0), and it gets larger at larger pointing angle. The RPC model used in this study is the model for odd detectors because transform coefficients recorded in leader file is for odd detectors. For even detectors, the offset that is a function of pointing angle is added in this study.

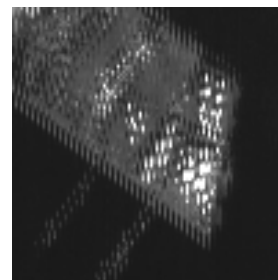


Fig. 3 Staggered arrayed detector of AVNIR-2

Geometric accuracy of AVNIR-2 product is assessed by the comparison of image position with GCPs. Reference data are 1:2500 digital map in order to get the position of ground features (road, river and sea bank), 50 meters grid DEM and 2 kilometers grid geoid data for height derivation, respectively. These data are maintained by Geographical Survey Institute of Japan, and can be freely downloaded via Internet. Corresponded features were selected from AVNIR-2 and digital map using GCP collection tools (figure 4). Latitude and longitude are derived from digital map, and height from the earth ellipsoid is from the sum of DEM and geoid. Line and pixel positions, which are calculated by RPC model using

latitude, longitude, and height, are compared with "correct" positions selected from AVNIR-2 image.

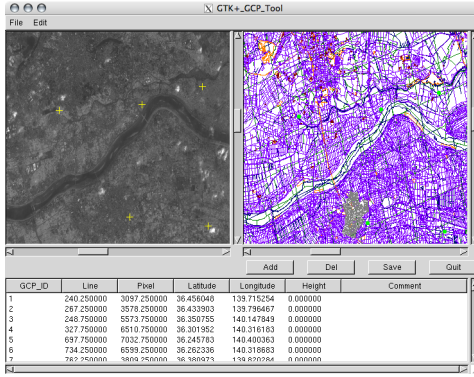


Fig. 4 GCP collection tool

The RPC model should be modified if there is geometric error. The modification is carried out using quasi-affine transformation written in equation 2. Where, l_r and p_r are image position derived by RPC model, l_m and p_m are those of GCP, respectively. a_i and b_i ($i = 0,1,2,3$) are the coefficients estimated by least squares regression. Image position (line, pixel) at the height of 0 meter, which is derived at first process of above mentioned step 2, is modified using this equation, then RPC model is re-calculated using modified ground position.

$$\begin{bmatrix} l_m \\ p_m \end{bmatrix} = \begin{bmatrix} a_0 & a_1 & a_2 & a_3 \\ b_0 & b_1 & b_2 & b_3 \end{bmatrix} \begin{bmatrix} l_r \\ p_r \\ 1 \end{bmatrix} \quad (2)$$

3.2 Land cover classification

Land cover monitoring is one of the important missions of ALOS, and multispectral image of AVNIR-2 has an ability to produce the land cover map with higher spatial resolution and extensive spatial coverage. Land cover classification of higher spatial resolution has an advantage of availability of spatial (texture) information of pixels, compared to that of moderate resolution sensors such as Landsat TM. Land cover classification in this study is implemented the sequence of image segmentation, decision tree classification and post-processing.

Image segmentation is based on region growing approach [5]. The key concept of the method is that pixels that have similar spectral characteristics were merged to form the groups of the pixels (segments or regions). All pixels are initially considered to be seed of the segments in this study, and then two adjacent segments that have lowest score among the adjacent segments, i.e. most similar neighboring segments, will be merged while score is lower than threshold. Score is calculated by the weighted sum of spectral score and spatial score as shown in equations 3. The spectral score is the band-averaged

difference of the average digital number (DN) of the segments. This compares the spectral similarity of the two segments. The spatial score evaluates the shape of the merged segments. Since the score becomes lower in case of smoother segment, a pair of segments that has smoother shape in post-merged segment will be merged preferentially. Control parameters of segmentation are weight of spectral score and termination threshold of score.

$$Score_{i,j} = \omega \cdot SpectralScore_{i,j} + (1 - \omega) SpatialScore_{i,j} \quad (3-a)$$

$$SpectralScore_{i,j} = \sqrt{\frac{1}{B} \sum_{b=1}^B (a_{i,b} - a_{j,b})^2} \quad (3-b)$$

$$SpatialScore_{i,j} = L_{(i+j)} - P_{(i+j)} \quad (3-c)$$

where

ω : Weight of spectral score (0 to 1)

B : Number of band of AVNIR-2 (=4)

a_b : Average of digital number in band

$L_{(i+j)}$: Perimeter of merged segment of i and j

$P_{(i+j)}$: Perimeter of bounding box of merged segment

i, j : Indices of segment

The purpose of this classification is forest type identification, therefore land covers are 7 classes as primary forest, secondary forest, slash-and-burn agriculture, bare ground (road and logged area), water, cloud and shadow (of cloud and mountain). A hundred of training segments are selected for each class except slash-and-burn (70 segments) from the segmented image by the visual interpretation. The structure, criteria, and threshold values of decision tree classification were decided based on these training segments manually according to the scatter diagram of segment statistics (figure 5 for example) and trial classifications. The availability of the standard deviation of the pixels within the segment is tested as the metric of the classification, but no clear aptitude is derived. Flow of decision tree classification used in this study is shown in figure 6.

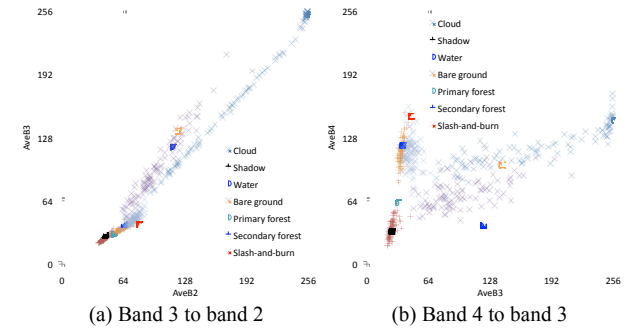


Fig. 5 Scatter plot of average DN of training segments

Post classification was achieved to modify the misclassification around the cloud area. The reflectance (of land feature) is a little higher at the edge of the cloud

due to the interference of thin cloud. Therefore, Bare ground and slash-and-burn that adjacent to cloud were modified to cloud and secondary forest, respectively. Then, water which adjacent to cloud and shadow was modified to shadow.

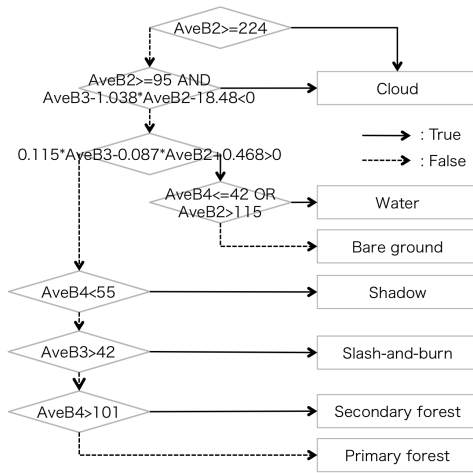


Fig. 6 Flow of decision tree classification

4. RESULTS AND DISCUSSIONS

4.1 Generation of RPC model

The RPC before and after correction for the product with the pointing angle of 0.0 are shown in table 2. The scatter plot of error for all products are shown in figure 7. Errors were relatively larger in the pixel (across track) direction than line (along track) direction of the image. There is no clear trend along with the pointing angle, but the scene with larger error in the pixel direction has also the larger error in the line direction. Root mean square errors are 5.44, 4.05, 6.40, 9.18 pixels along with pointing angles before correction. These errors were reduced to 0.87, 0.86, 0.78 and 0.94 respectively after the modification (numbers of sample are 88, 117, 195 and 190). All errors were reduced to less than one pixel. The residuals are mainly owing to the instability of the visual interpretation of GCPs at the collection process rather than errors of product. The GCPs were selected from gray scale image of band 3, because level 1B1 product is not corrected for the band-to-band registration. Therefore, it was difficult to pick up the image points, compared with the case of color composite image. Geometrically rectified images around bay of Chiba area overlaid by digital map are shown in figure 8. It is clear on the shoreline of harbor that error was corrected especially in horizontal direction.

The geometric accuracy of AVNIR-2 is relatively lower than that of PRISM, and this seems due to the alignment and control of pointing mirror. It means that scene-based correction using GCPs is necessary for AVNIR-2. As a result of the modification of RPC using reference map and DEM, the errors were modified to less than one pixel in all products of this study. However, it should be noted about the correction of RPC of this study

that accuracy of the correction depends on the distribution of GCPs in the scene as in the case with another geometric correction method. Since the modification of the RPC is based on the quasi-affine transformation using GCPs, the coefficients are extrapolated all over the scene and elevation even if there is no GCP in some area or in some height. This has an underlying risk of low geometric accuracy of correction, especially in the mountainous region where is low contrast, high elevation, less GCP compared with urban and agricultural area. Automatic GCP matching with PRISM data is one of the countermeasures against it. Additionally, digital surface model derived from PRISM is also effective to get the height of the GCPs.

Table 2 RPC for the product ALAV2A058492880

(a) Before correction					(b) After correction				
	N_l	D_l	N_p	D_p		N_l	D_l	N_p	D_p
C_0	-7.10E-05	1.00E+00	4.61E-03	1.00E+00	C_0	6.46E-04	1.00E+00	3.03E-03	1.00E+00
C_1	-2.48E-01	-1.03E-02	1.21E+00	1.99E-03	C_1	-2.48E-01	-6.07E-03	1.21E+00	2.00E-03
C_2	-1.14E+00	5.18E-05	-3.06E-01	5.88E-03	C_2	-1.14E+00	-2.87E-03	-3.06E-01	5.90E-03
C_3	-4.91E-04	-4.49E-03	7.75E-05	-1.43E-03	C_3	-4.95E-04	-6.75E-03	7.97E-05	-1.43E-03
C_4	1.37E-02	1.36E-04	6.47E-05	1.70E-05	C_4	9.57E-03	5.74E-04	5.92E-05	1.55E-05
C_5	1.12E-03	1.16E-04	7.92E-03	-4.79E-05	C_5	1.68E-03	1.93E-04	7.92E-03	-4.82E-05
C_6	5.14E-03	5.49E-04	-2.01E-03	1.17E-04	C_6	7.72E-03	9.11E-04	-2.01E-03	1.17E-04
C_7	8.07E-05	-2.00E-04	1.67E-03	-2.20E-04	C_7	-9.72E-04	-1.61E-04	1.67E-03	-2.19E-04
C_8	-2.78E-04	4.11E-04	-1.41E-03	-5.40E-05	C_8	3.06E-03	1.66E-03	-1.41E-03	-5.31E-05
C_9	2.60E-06	-1.31E-06	2.71E-07	-4.59E-05	C_9	3.71E-06	-1.17E-06	3.43E-07	-4.59E-05
C_{10}	-2.77E-04	8.55E-07	1.64E-04	1.73E-06	C_{10}	-4.60E-04	1.44E-06	1.65E-04	1.74E-06
C_{11}	7.39E-05	2.31E-07	-1.62E-04	-6.68E-08	C_{11}	5.37E-05	-1.87E-07	-1.61E-04	-6.70E-08
C_{12}	-2.42E-04	9.60E-07	-2.07E-04	1.56E-08	C_{12}	-1.06E-03	2.98E-06	-2.05E-04	8.49E-09
C_{13}	2.59E-07	-2.04E-10	1.81E-07	2.73E-07	C_{13}	1.87E-07	9.70E-10	1.79E-07	2.75E-07
C_{14}	1.64E-04	-4.76E-07	-3.41E-05	9.48E-07	C_{14}	2.57E-05	-2.81E-06	-3.61E-05	9.49E-07
C_{15}	-4.73E-04	-2.56E-07	-1.14E-04	-6.80E-07	C_{15}	-1.90E-03	-4.96E-07	-1.14E-04	-6.78E-07
C_{16}	1.23E-06	3.78E-10	-4.46E-08	-1.26E-06	C_{16}	9.04E-07	2.03E-09	-4.24E-08	-1.26E-06
C_{17}	-1.75E-05	-1.14E-06	-4.39E-05	-2.09E-06	C_{17}	-3.11E-05	-1.89E-06	-4.42E-05	-2.10E-06
C_{18}	-6.27E-04	-8.95E-08	-4.75E-05	1.12E-06	C_{18}	-1.04E-03	-1.60E-07	-4.76E-05	1.12E-06
C_{19}	-1.75E-09	1.77E-10	-3.72E-11	3.53E-08	C_{19}	-2.90E-09	2.76E-10	-9.09E-11	3.53E-08

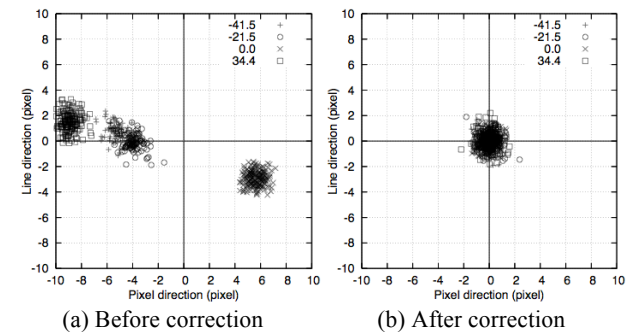


Fig. 7 Geometric errors



Fig. 8 Geometrically rectified images

4.2 Land cover classification

Segmented images by two extreme cases of the weight of spectral score are shown in figure 9. In the case of ω equals 1.00, the size and shape of the segments have larger variation because segmentation was achieved only by spectral information and spatial score is not taken into account. In ω equals 0.01, on the other hands, segments have similar sizes and smooth shapes, though there are several mixed segments of forest with water. This is due to the higher weight to the spatial score. Final classification was achieved using ω of 0.60 as a result of several trials by applying different ω .

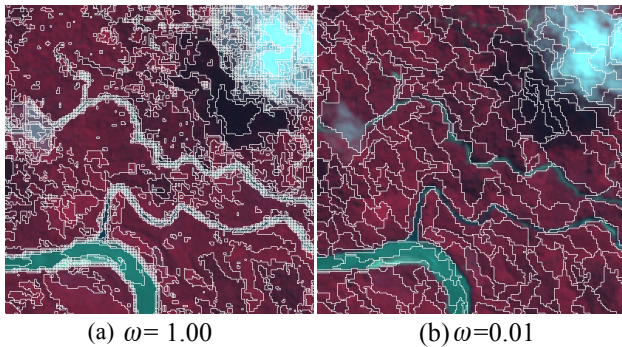
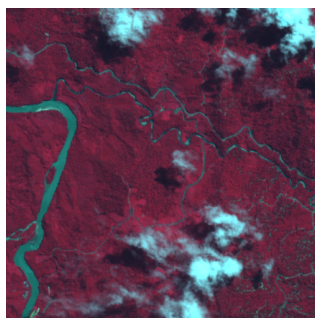
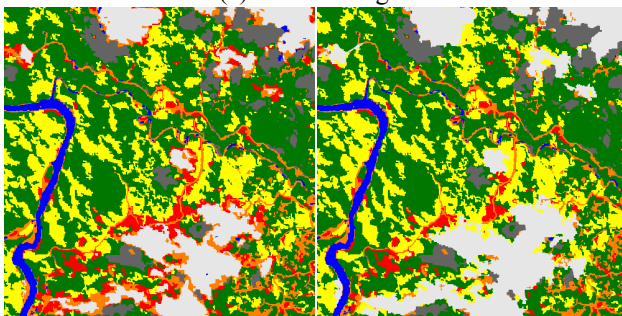


Fig. 9 Segments by the weight of spectral score



(a) Source image



(b) Before

(c) After

Fig. 10 Post-classification

The advantage of post-classification is shown in figure 10. The segments on the edge of cloud were misclassified to bare ground or slash-and-burn agricultural classes due to the slight increase of the reflectance by the coverage of thin and transparent cloud. These segments were reclassified to cloud and secondary forest by the post-

classification, respectively. There is little chance to get the cloudless images by optical sensors, especially over the tropical regions, hence provision for the cloud (and its shadow) is important issue of the land cover classification.

Figure 11 shows 2 partial areas in the image, where located inland of the Sarawak state, Borneo island. Large area is covered by primary forest. The secondary forest and slash-and-burn agricultural area are distributed along the road (classified as bare ground). The main difference between secondary forest and slash-and-burn is small difference of reflectance. Slash-and-burn region has a slightly higher reflectance in band 3 (red region of wavelength) compared with secondary forest. This might be referred from the form of the land surface and vegetation. Secondary forest is composed of woody type of vegetation and density of the leaves is higher. On the contrary, slash-and-burn agricultural area is composed mainly of herbaceous plant and leaf density is low.

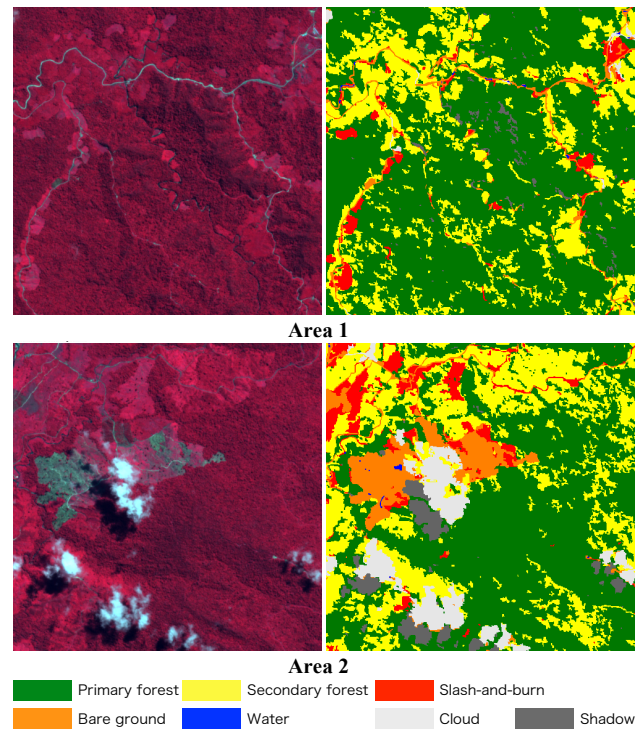


Fig. 11 Source and classification image (partial areas)

Large bare ground in area 2 is the logged forest for the plantation. Timbers were clear-cut for the preparation to plant the oil palm for oil, or acacia for timber production. The plantations around the logged area are classified to the secondary forest or slash-and-burn agricultural area in this classification. However, larger patches of slash-and-burn located in northwestern part of the image seem to be the misclassification. The early stage of the plantation might have similar spectral characteristics because it is composed of woods of lower height and density. The reflectance of land surface with this condition is comparable to that of slash-and-burn area. The utilization

Table 3 Contingency table of the classification

		Classification							Total	P's Acc.
		Primary F.	Secondary F.	Slash-&-burn	Bare Ground	Water	Cloud	Shadow		
Training segment	Primary Forest	73	26	0	0	0	0	1	100	73.0
	Secondary Forest	12	86	2	0	0	0	0	100	86.0
	Slash-and-burn	1	23	41	4	0	1	0	70	58.6
	Bare Ground	0	0	1	67	26	6	0	100	67.0
	Water	2	3	0	19	68	0	8	100	68.0
	Cloud	0	0	0	1	0	99	0	100	99.0
	Shadow	2	0	0	0	0	0	98	100	98.0
	Total	90	138	44	91	94	106	107	670	Overall
User's Acc.	81.1	62.3	93.2	73.6	72.3	93.4	91.6		79.4	

of size of segment as the classification metrics is proposed measures for this issue.

Contingency table of the classification is shown in table 3. The table usually should be made using the validation area in general, however the training area for the classification is used in this study because of difficulty in the acquisition of validation data. Overall accuracy is around 79%. The major misclassifications are between primary forest and secondary forest, secondary forest and slash-and-burn, and bare ground and water. The reason of misclassification of primary forest and secondary forest is that it is difficult to discriminate clearly because these are continuous stage of the ecological succession of forest. For the secondary forest and slash-and-burn area have similar characteristics as mentioned above. The reason of the misclassification of bare ground and water is the muddy stream of the river water. The color of the river water is brownish in this area caused by interfusion of soil. The similar spectral characteristics of these classes result in misclassification.

Lowest producers accuracy is in slash-and-burn of about 59%, and highest is secondary forest of 86% except cloud and shadow. For users accuracy is highest in slash-and-burn (93%), and lowest in secondary forest (62%). It seems that there is a trade-off between two accuracies.

5. CONCLUSIONS

Geometric calibration of AVNIR-2 was achieved using self-generated RPC model. The geometric accuracy of AVNIR-2 is around several pixels and it depends on the scene (i.e. pointing angle setting). Therefore, scene-based geometric correction based on ground control points is necessary at this moment. PRISM image is one of the functional reference data used as GCPs, since it has higher accuracy and frequently operated simultaneously with AVNIR-2. The re-processing of AVNIR-2 in combination with higher geometric correction is prospective in the future.

Land cover classification was experimented over tropical forest. Decision tree classification using image segment is effective method due to the higher spatial resolution of AVNIR-2. Though further improvement in segmentation and construction of the decision tree are needed, AVNIR-2 has a great potential of land cover classification not only with higher spatial resolution, but

also wider spatial coverage. One capability of higher classification accuracy is utilization of fused (pan-sharpened) image of AVNIR-2 with PRISM.

ACKNOWLEDGEMENT

This research is conducting as a part of Research Announcement (RA) of ALOS Science Program.

REFERENCES

- [1] Tadono T., "Results of Initial Calibration and Validation of PRISM and AVNIR-2", http://www.eorc.jaxa.jp/ALOS/kyoto/jan2007/pdf/1-04-Tadono_KC7.pdf. (accessed on 15th, May 2008)
- [2] Geospatial Intelligence Standards Working Group, "The Compendium of Controlled Extensions (CE) for the National Imagery Transmission Format (NITF) (version 3.0), Appendix E Airborne Support Data Extensions (ASDE) (version 2.1)", 2007, http://www.gwg.nga.mil/ntb/baseline/docs/stdi00021/stdi0002_v30/index.html. (accessed on 15th May 2008).
- [3] Tao, C., V., and Hu, Y., "A Comprehensive Study of the Rational Function Model for Photogrammetric Processing", *Photogrammetric Engineering and Remote Sensing*, Vol. 67, No. 12, pp. 1347-1357, 2001.
- [4] Earth Observation Research and Application Center, Japan Aerospace Exploration Agency, "ALOS Data Users Handbook (draft version)" (in Japanese), 2004.
- [5] C. B. Ursula, H. Peter, W. Gregor, L. Iris, and H. Heynen, "Multi-resolution, object-oriented fuzzy analysis of remote sensing data for GIS-ready information," *JISPRS Journal of Photogrammetry & Remote Sensing*, 58, pp. 239-258, 2004.